Geophys. J. Int. (2004) **158,** 729–743 doi: 10.1111/j.1365-246X.2004.02311.x

Temperature and melting of a ridge-centred plume with application to Iceland. Part I: Dynamics and crust production

T. Ruedas,* H. Schmeling, G. Marquart,† A. Kreutzmann and A. Junge

Institute of Meteorology and Geophysics, J. W. Goethe University Frankfurt, Feldbergstrasse 47, D-60323 *Frankfurt am Main, Germany*

Accepted 2004 March 5. Received 2004 January 5; in original form 2003 February 10

SUMMARY

In this study and a companion paper, numerical models of convection and melt generation in a ridge-centred plume system are developed for plumes with different temperature anomalies ΔT_P and varying fractions of retained melt φ_ex. The produced melt in excess of the retention threshold is used to generate ridge and plume crust respectively, whose thickness is found to be sensitive to changes in ΔT_P and φ_ex. Comparison of calculated crustal thicknesses with observations from mid-oceanic ridges and from Iceland confirms earlier findings that ΔT_P of the Iceland plume in the upper mantle is about 150–200 K and that the Icelandic crust is thick. It also suggests that the retained melt fraction in partially molten mantle is at most 1 per cent. In the preferred model, plume melting occurs between ca. 25 and 110 km depth, at up to ∼250 km from the spreading centre. The temperature and melt fraction fields from the numerical models are used as input for the derivation of seismic velocity anomalies and magnetotelluric response functions in the companion paper. Furthermore, the models reveal that the high temperatures of plumes result in a superlinear increase of crustal thickness with plume excess temperature through the combined effects of enhanced melting, active upwelling and the extent and geometry of the melting zone.

Key words: hotspots, Iceland plume, mantle convection, melt, mid-ocean ridges, numerical modelling.

1 INTRODUCTION

Mid-oceanic ridges and plumes are two central elements of plate tectonics and play prominent, though different, roles in igneous petrogenesis and crust formation. While at mid-ocean ridges, the newly created crust in general is of a rather uniform thickness of 6–7 km throughout the world (e.g. White *et al.* 1992), plumes vary considerably in strength, and their crust production depends very much on their excess temperature, i.e. their temperature contrast with respect to undisturbed mantle, and on the thickness of the overlying lithosphere. In the exceptional case where a plume coincides with a ridge, it can unfold the capacity for melt production provided by its high temperature to the maximum extent without being oppressed and weakened by a thick lithospheric lid. Currently, this situation is realized in Iceland, where the superposition of a mantle plume with the mid-Atlantic ridge has allowed for the ridge crest to grow above sea level and form an island. For this unique situation Iceland has received much interest since the development of the plume paradigm (Morgan 1971), and has indeed been regarded by many workers (e.g. Courtillot *et al.* 2003) as one of the classical and best-documented examples of a deep mantle plume. The presence of a strong anomaly in the upper mantle has been confirmed by many studies, such as several regional seismic tomography experiments (Tryggvason *et al.* 1983; Wolfe *et al.* 1997; Allen *et al.* 1999, 2002a; Foulger *et al.* 2001), receiver function analysis (Shen *et al.* 2002) or regional geoid analysis (Marquart 1991). The shape and strength of the plume in the deeper mantle, which is essentially determined by global seismic tomography, is less well resolved. This has led some authors to the claim that the plume is restricted to the upper mantle (e.g. Foulger *et al.* 2001), but several recent tomographic studies are able to trace a rather narrow structure of varying amplitude from below the Iceland area down to the core–mantle boundary (Bijwaard & Spakman 1999; Ritsema *et al.* 1999; Zhao 2001; Grand 2002). Furthermore, a number of geochemical studies have also found evidence for the presence of lower-mantle material in the plume (e.g. Hanan & Schilling 1997; Hanan *et al.* 2000; Kempton *et al.* 2000; Breddam 2002).

A different point of controversy is the thickness of the crust above this mantle anomaly. Symptomatic of this issue are contradictory results from controlled-source seismic experiments performed around 1980: the results of the RRISP77 campaign (Gebrande *et al.* 1980) indicated that the crust is as thin as 10 km near the ridge, whereas

*Now at: Dansk Lithosfærecenter, Øster Voldgade 10 L, 1350 Copenhagen K, Denmark. E-mail: tr@dlc.ku.dk

†Now at: Space Research Organization Netherlands & University of Utrecht, PO Box 80021, 3508 TA Utrecht, the Netherlands.

studies by Zverev *et al.* (1980a,b) imaged crustal reflectors at depths of at least 20 km. Later, reinterpretation of the RRISP data (Menke *et al.* 1996) and new seismic and gravity data (e.g. Bjarnason *et al.* 1993; Staples *et al.* 1997; Darbyshire *et al.* 1998) strengthened the evidence for a thick crust. However, magnetotelluric measurements, for example by Beblo & Björnsson (1980), showed unambiguously the presence of a good conductor at a depth of about 10 km near the ridge, which slopes to greater depth under older parts of the island. This conductor has then been interpreted as a layer of partial melts, which could only exist at the base of the crust in this form. Although alternatives have been proposed, the nature of this layer remains unclear and fuels the controversy about the structure of the Icelandic crust.

In this study, we attempt to contribute to the discussion by developing a numerical convection model of a ridge-centred plume in the upper mantle such as in Iceland and combining it with a model of melt generation and segregation from which we compute crustal thickness; the restriction to the upper mantle is dictated by computational limitations and is also motivated by the availability of high-resolution seismic data, but the design of the model in fact assumes that the plume ascends from the lower mantle. Furthermore, the numerical model delivers the geometry of the temperature and melt content fields in the mantle, which can be used as input for calculations of seismic velocity anomalies and the distribution of the electrical conductivity in the mantle on the basis of theoretical models of the effect of temperature and melt on these observables (Schmeling 1985, 1986; Karato 1993). These aspects are the subject of a companion paper by Kreutzmann *et al.* (2004) (hereafter referred to as Paper 2). The sensitivity to temperature and melt content of all observables considered is our rationale for concentrating on variations of these two parameters. Hence, it extends the picture developed in the earlier numerical work of Ribe *et al.* (1995), in which only two models were dedicated especially to Iceland, and of Ito *et al.* (1996) and Ito *et al.* (1999), which mainly concentrated on gravity and chemical anomalies apart from crustal thickness. The combination of the results of Paper 2 with those of this study will improve the view of the Icelandic mantle and crust, linking constraints on mantle structure to observations of the thickness of the crust and also exploring new possibilities for probing the structure of the uppermost mantle.

2 DYNAMIC MODELLING OF A RIDGE-CENTRED PLUME

2.1 Model design

The idealized numerical model of the Iceland plume used in this study consists of a ridge-centred plume in a 3-D Cartesian box and comprises two parts. First, there is a large-scale model which treats the convection of the plume and the mantle flow in its greater neighbourhood in the depth range of the upper mantle. The plume is defined as entering the corresponding model box through a circular area in the bottom of the model, which is characterized by a temperature and vertical flow velocity anomaly. Obviously, melting takes place only in a minor part of this large-scale model, namely in the surroundings of the spreading centre and the plume axis in the upper quarter of the box. Therefore, it is natural to restrict the other part of the model, the modelling of the melting processes, to this smaller region, which is represented on a more densely sampled Cartesian grid inserted into the large-scale box.

2.1.1 *Governing equations for mantle and melt processes*

In the large-scale mantle convection model, two equations are solved. The first one is the incompressible Stokes equation for infinite Prandtl number in the Boussinesq approximation:

$$0 = -\nabla \tilde{p} + \nabla \cdot \left\{ \eta \left[\nabla \mathbf{v}_\mathrm{s} + (\nabla \mathbf{v}_\mathrm{s})^\mathrm{T} \right] \right\} + g(-\varrho_0 \alpha T + \Delta\varrho_\mathrm{dp} f + \Delta\varrho_\mathrm{f} \varphi + \Delta\varrho_X X)\mathbf{e}_z, \quad (1)$$

with the non-hydrostatic pressure $\tilde{p}$, the mantle flow velocity $\mathbf{v}_\mathrm{s}$, and the mantle shear viscosity η (see Table 1 for a complete list of variables). The four terms in the round brackets characterize the contributions of thermal expansion α, depletion due to melting f, retained melt (porosity) φ and the phase transformations from α-olivine to γ-olivine X to the buoyancy of the upwelling material (see e.g. Schmeling 2000); $\Delta\varrho_\mathrm{dp}$, $\Delta\varrho_\mathrm{f}$, and $\Delta\varrho_X$ are density contrasts between undepleted mantle and mantle at a reference f, between melt and matrix, and between the two phases involved in a solid state phase transition, respectively.

The second equation is the energy conservation equation:

$$\frac{\partial T}{\partial t} = \kappa \nabla^2 T - \mathbf{v}_\mathrm{s} \cdot \nabla T + \frac{g\alpha}{c_p} \overline{T} v_{\mathrm{s}_z} + \frac{\eta}{2\varrho_0 c_p} \left[\nabla \mathbf{v}_\mathrm{s} + (\nabla \mathbf{v}_\mathrm{s})^\mathrm{T} \right] \cdot \left[\nabla \mathbf{v}_\mathrm{s} + (\nabla \mathbf{v}_\mathrm{s})^\mathrm{T} \right] - \frac{L_\mathrm{m}}{c_p} \left(\frac{\partial}{\partial t} + \mathbf{v}_\mathrm{s} \cdot \nabla \right) M + \overline{T} \frac{\Delta S_X}{c_p} \left(\frac{\partial}{\partial t} + \mathbf{v}_\mathrm{s} \cdot \nabla \right) X, \quad (2)$$

with the temperature T and the melt mass M produced by supersolidus melting. The third and fourth terms represent adiabatic and viscous heating, respectively, and the last two terms describe the temperature changes due to the consumption of latent heat during melting and solid state phase transitions, respectively. Both equations are actually solved in the modelling of mantle convection in non-dimensionalized form. Note that α is depth dependent; the depth dependence, which is detailed in Paper 2, results in a drop of α by about 44 per cent over the depth range of the model (*cf.* Table 1). The transitions from α-olivine to γ-olivine are assumed to happen linearly over a depth range of about 100 km. The plagioclase–spinel and the spinel–garnet transition of the principal Al-bearing phase are not included, because the relatively small T decrease associated with them will have only a minor effect on the temperatures in the melting region and hence on the degree of melting and the observables considered here, and the density change of about 30 kg m^{-3} for the spinel–garnet transition (e.g. Cella & Rapolla 1997) is not expected to enhance the buoyancy of the plume substantially either, contrary to the buoyancy effect in the transition zone (see Section 2.2).

In the smaller-scale model grid, the dynamics of melt generation and migration in a compacting, porous matrix are calculated after the method derived by McKenzie (1984) and implemented for the 2-D case in an earlier work by Schmeling (2000); the relevant mechanisms are the advection of the depletion respectively the degree of melting f by the mantle current,

$$\left(\frac{\partial}{\partial t} + \mathbf{v}_\mathrm{s} \cdot \nabla \right) f = \frac{1}{\varrho_\mathrm{f}} \left(\frac{\partial}{\partial t} + \mathbf{v}_\mathrm{s} \cdot \nabla \right) M, \quad (3)$$

the conservation of melt mass,

$$\frac{\partial (\varrho_\mathrm{f} \varphi)}{\partial t} + \nabla \cdot (\varrho_\mathrm{f} \varphi \mathbf{v}_\mathrm{f}) = \left(\frac{\partial}{\partial t} + \mathbf{v}_\mathrm{s} \cdot \nabla \right) M, \quad (4)$$

Table 1. Variables used in this study, and model parameters; values in italics are characteristic of the reference model DPRM. For better computational efficiency, z_m was varied for different ΔT_P, because the respective plumes cross the solidus at different depths; therefore a hotter plume needs a melt model grid which reaches deeper into the mantle.

Variable	Unit or value
General	
η, mantle shear viscosity	Pa s
φ, porosity (melt content)	
a, grain size	1 mm
b, permeability scaling parameter	648
$\mathbf{e}_z$, unit vector in z direction	
f, depletion (melting degree)	
g, gravity acceleration	9.9 m s^{-2}
h, crustal thickness	km
k_φ, permeability	m^{-2}
$\tilde{p}$, dynamic pressure	GPa
T, temperature	°C
$\overline{T}$, absolute temperature	K
$\tilde{T} = [T - 0.5(T_s + T_l)]/(T_l - T_s)$, homologous temperature	
T_s, solidus temperature	°C, eq. (8)
T_l, liquidus temperature	°C, eq. (9)
$\mathbf{v}_f$, fluid (melt) velocity	cm yr^{-1}
$\mathbf{v}_s$, solid (matrix) velocity	cm yr^{-1}
$\mathbf{v}_{seg} = \mathbf{v}_f - \mathbf{v}_s$, segregation velocity	cm yr^{-1}
X, normalized fraction of a certain olivine polymorph	
Δz_X, depression of the 410 km discontinuity	km
z_{sol}, solidus depth	km
Model	
x_c, y_c, z_c, size of convection model	1500 km × 1000 km × 660 km
x_m, y_m, z_m, size of melt model	556 km × 1000 km × (113, *127*, 153) km
$\Delta T_P(z_c)$, plume excess temperatures at model bottom	150 K, *250* K, 350 K
φ_{ex}, extraction threshold	0.001, *0.01*, 0.03, (1)
$r_P(z_c)$, plume radius at model bottom	125 km
$v_{z,P}(z_c)$, max. vertical bottom influx velocity of plume	3 cm yr^{-1}
v_r, half-spreading velocity	1 cm yr^{-1}
Mantle	
α, thermal expansivity	(4.27–2.39) × 10^{-5} K^{-1}
η_0, reference shear viscosity	5 × 10^{22} Pa s
η_b, bulk viscosity	5 × 10^{21} Pa s
κ, thermal diffusivity	6.072 × 10^{-7} m^2 s^{-1}
ϱ_0, reference density	3660 kg m^{-3}
c_p, isobaric specific heat	1350 J kg^{-1} K^{-1}
ΔS_X, entropy change of phase transformation	53.8 J kg^{-1} K
T_{pot}, background mantle potential temperature	1380, *1410* °C
X_{ol}, fraction of olivine	0.65
Melt	
α_f, thermal expansivity	6.3 × 10^{-5} K^{-1}
η_f, viscosity	2 Pa s
$\varrho_{0,f}$, reference density	2663 kg m^{-3}
K_0, K_0', bulk modulus and p derivative	22.3 GPa, 7
L_m, latent heat of melting	550 kJ kg^{-1}
M, melt production	kg m^{-3}

where melting/freezing is included, and the relative motion of melt and matrix under the influence of melt buoyancy, deviatoric stresses and compaction, in the compaction Boussinesq approximation (Schmeling 2000),

$$\mathbf{v}_f - \mathbf{v}_s = \frac{\Delta\varrho_f g a^2}{\eta_f b}\varphi^{n-1}(1-\varphi)\mathbf{e}_z - \frac{a^2}{\eta_f b}\varphi^{n-1}\nabla\cdot\left\{\eta\left[\nabla\mathbf{v}_s + (\nabla\mathbf{v}_s)^T\right] + \eta_b(\nabla\cdot\mathbf{v}_s)\right\}. \quad (5)$$

The factors on the right-hand side are related to the well-known porosity–permeability relation:

$$k_\varphi = \frac{a^2\varphi^n}{b}; \quad (6)$$

we chose 1 mm for the grain size a and assumed a geometry factor $b = 648$ and $n = 3$, which is valid for a network of planar layers.

We did not solve the energy equation in a formulation for two-phase flow as given by McKenzie (1984), because we imposed an upper limit to the porosity in the mantle which is rather low

and extracted all melt exceeding this threshold instantaneously, as described in the next section. Therefore, the segregation velocities in the two-phase flow are slow enough to allow us to approximate the average velocity of the melt–matrix system by the matrix velocity, which implies that thermal equilibrium prevails between both phases and that the dissipation due to the relative movement of melt and matrix is negligible (*cf.* Schmeling 2000). Furthermore, the removal of excess melt from the system in principle entails the extraction of energy from it. Assuming equal heat capacity and density of melt and matrix, this energy loss would be compensated by the advection of heat due to matrix compaction. As we neglect this compaction term in the compaction Boussinesq approximation, it is consistent to neglect the extraction of energy as well. The only cooling mechanisms acting in the melting region are therefore those due to adiabatic ascent and the consumption of latent heat by melting, as described above.

2.1.2 Numerical method

In the large-scale convection model, the Stokes eq. (1) is solved by a hybrid Fourier/finite difference method (Marquart *et al.* 2000; Marquart 2001), whereas the energy conservation eq. (2) and the melt dynamic eqs (3), (4) and (5) for the small-scale melt grid are all solved with pure finite differences. Time stepping is performed by an explicit integration method, allowing for a detailed examination of the transient phases of plume ascent; the same time increment is used on both numerical grids. To achieve a higher resolution for the investigation of melt-related processes, the spatial discretization of the melt model is higher than that of the convection model; the physical variables which are of importance in both models—T, $\mathbf{v}_\mathrm{s}$, η, f and φ—are exchanged by interpolation, respectively by selection, of a value at common points (the refinement factor is always an integer). For the convection model, which has a size of 1500 km × 1000 km × 660 km, a grid of 108 × 72 × 100 points has been found to be sufficient according to resolution tests; the melt grid, which for the reference case is of size 556 km × 1000 km × 127 km and is situated along the ridge in the depth interval from 6.7 to 133 km, consists of 121 × 214 × 20 points, i.e. it is more densely sampled by a factor of 3 in the x and y directions compared with the convection grid and thus has an approximately uniform resolution in all directions; its depth and gridpoint number are adopted to the depth range of melting for each model.

The temperature is held at a constant value of 0 °C at the top of the model and of 239 K above the potential temperature of the model at the bottom outside the plume. As mentioned above, the plume source is prescribed at the model bottom as a circular area with radius $2r_\mathrm{P}$ featuring a temperature anomaly and a vertical influx of a maximum 3 cm yr^{-1}, both weighted with the same Gaussian shape, because as the buoyancy is largest and the viscosity is lowest in the hottest parts of the plume it is consistent to assume similar patterns for T and v_z in the source region; r_P is the distance from the centre at which the amplitude of the anomaly has decreased to $1/\mathrm{e}$. Apart from that, there is a weak background influx related to the passive upwelling current. To balance the influx of mass, two strips oriented perpendicularly to the spreading direction are provided at the outer sides of the bottom of the model to take up the entire mass input. At the top of the model, the spreading ridge is implemented as a kinematic boundary condition; plate velocities change linearly across the region of the spreading centre over a width of 60 km, but have the constant value of v_r outside of that area. The lateral boundaries are periodic.

The rheology of the mantle was chosen to be temperature- and depth-dependent according to $\eta(T, z) = \eta_0 \exp(-c_T T + c_z z)$ with $\eta_0 = 5 \times 10^{22}$ Pa s, $c_T = 6.908$ and $c_z = 2.7$. This leads to viscosity variations of $O(10^3)$, which approaches the limit of what can be treated accurately with the present method. In normal mantle, viscosities hence reach minimum values around (6–7.5) × 10^{19} Pa s at asthenospheric depths, but rise to about (1.2–2.2) × 10^{20} Pa s in the transition zone and η_0 at the surface; in the depth range of the phase transition, the pressure effect and the increase of superadiabatic temperature with depth roughly compensate each other, resulting in a vertically almost constant viscosity profile in that interval. The factor η_b in the compaction term of eq. (5) is the bulk viscosity of the partially molten rock; it is assumed constant here for simplicity, but its actual dependence on porosity (Schmeling 2000; Bercovici *et al.* 2001) would not play a significant role at the porosities prevailing in the models presented here, as the porosity distribution is quite homogeneous in the models.

The generation of oceanic crust is modelled by extracting instantaneously all melt exceeding a certain threshold melt content φ_ex in ridge-perpendicular (x–z) planes after each time step and adding it uniformly to the top of the model in a spreading and eruption zone with a width of 60 km, from where it is transported laterally by the plate motion. The corresponding transport equation describing the crustal thickness h,

$$\frac{\partial h}{\partial t} + \frac{\partial (h v_\mathrm{r})}{\partial x} = \mathcal{E} \tag{7}$$

(after Buck 1991), is solved by finite differences on a 2-D grid with the same spatial sampling as the melt grid; $\mathcal{E}$ is an 'eruption/intrusion rate'. The assumption of melt migration essentially perpendicular to the ridge is considered an acceptable approximation to the actual segregation (see also e.g. Ribe *et al.* 1995), and the instantaneous extraction reflects the fast transport of melt through some kind of oriented channel, which has been proposed by several authors (e.g. Stevenson 1989; Aharonov *et al.* 1995) and is also required by geochemical constraints (e.g. Lundstrom 2000). The direct modelling of channel formation and transport has, however, not been possible even with the finer discretization because of computational restrictions. On the other hand, focusing of melt by porous flow alone, while in fact occurring, is not very efficient, because porous flow is rather slow and the viscosity in the melting zone, which is around 5×10^{19} Pa s, is too low to produce large enough non-hydrostatic pressure gradients, as already concluded earlier by Phipps Morgan (1987) for a corner flow model.

2.1.3 Parametrization of melting behaviour

In view of the fact that a substantial amount of melt is generated within a few tens of degrees above the solidus, the choice of the potential temperature of the mantle and the solidus function is crucial. In view of the lack of melting experiments on mantle rock from beneath Iceland, it seems appropriate to choose a solidus T_s derived from an average mantle composition; a very recently published such parametrization is the one by Hirschmann (2000, table 2, and personal communication)

$$T_\mathrm{s} = 1120.66061 + 132.899012p - 5.1404654p^2, \tag{8}$$

with p in GPa and T_s in °C. The potential temperature T_pot of the mantle was generally assumed to be 1410 °C, which is high, though within the range of recent petrological estimates (Ryabchikov 1998; Green & Falloon 1998; Green *et al.* 2001) and results in a normal oceanic crust of about the thickness which is observed; such a need

Table 2. Model runs of this study. 135-1c is a variant of 135-1 with a background mantle potential temperature lower by 30 K.

Model	$\Delta T_P(z_c)$ (K)	ΔT_P(200 km) (K)	φ_{ex} (per cent)
DPRM (135-1)	250	136.5	1
220-1	350	220.5	1
50-1	150	52	1
135-0.1	250	136.5	0.1
135-3	250	136.5	3
135-100	250	136.5	100
135-1c	250	136.5	1

for higher potential temperatures has already been reported by other workers who also allowed for refreezing in models of convection and melt percolation (e.g. Ghods & Arkani-Hamed 2000). The degree of melting is described by the parametrization of melt fraction as a function of the homologous temperature $\tilde{T}$ by McKenzie & Bickle (1988), which seems to reproduce the melting degree for small to moderate f reasonably well and shows a decrease in productivity for $f \gtrsim 0.25$, as expected when clinopyroxene is going to be exhausted according to (batch melting) experiments (e.g. Hess 1992). Therefore we did not introduce an explicit 'clinopyroxene-out' discontinuity in our melting model. Even in the plumes f does not exceed this limit by very much, and it had been proposed that it might lie at higher degrees of melting in the case of fractional melting (Falloon *et al.* 1988, pp. 1273ff.). The actual degree of melting is determined by comparing the advected f with the theoretical degree of melting according to the homologous temperature using the parametrization, and melting or crystallizing according to the difference between both, taking into account the amount of melt locally available for possible freezing.

For the calculation of $\tilde{T}$, the liquidus of forsterite (the last solid phase in melting mantle rock) was used instead of the liquidus of lherzolite to mimic fractional melting in a similar manner as Iwamori *et al.* (1995); the parametrization of the mantle liquidus

$$T_l = 1718.15628 - 11.8091p + 187.91605\sqrt{p + 0.8} \quad (9)$$

was derived using data from several experiments on forsterite between 1 bar and 16.7 GPa (Davis & England 1964; Ohtani & Kumazawa 1981; Richet *et al.* 1993; Presnall & Walter 1993; Navrotsky 1994). As the melting curve of forsterite is at somewhat higher temperatures than the lherzolite liquidus, the parametrization of the degree of melting is stretched over a larger temperature interval at a given pressure, so that the isobaric productivity $(df/dT)_p$ is smaller, in agreement with predictions from incremental batch melting experiments (e.g. Hirose & Kawamura 1994). The smaller productivity also partly enforces the relatively high mantle temperature mentioned above.

2.2 Model runs

The initial condition for all models is a mantle with an adiabatic temperature–depth profile accounting for the depth dependence of α and the typical $\sqrt{t}$ shape of cooling oceanic lithosphere symmetrical to the spreading ridge, which is here prescribed in the form of the analytical solution to the problem (e.g. Turcotte & Schubert 1982). With this initial condition we miss the initial rifting and flood basalt phase of the opening of the ocean, but this is acceptable because we are mostly interested in the later stages of joint plume–ridge evolution, with regard to observables in the area of the present Iceland plume. The plume anomaly at the model bottom is characterized by $r_P = 125$ km, which is a value within the range of seismological studies (Tryggvason *et al.* 1983; Bjarnason *et al.* 1996; Wolfe *et al.* 1997; Foulger *et al.* 2001; Allen *et al.* 2002a), and a maximum influx velocity of 3 cm yr^{-1}, yielding a volume flux of 1.45 km^3 yr^{-1}, close to the 'best estimate' of Schilling (1991) of 1.43 km^3 yr^{-1}; however, the dynamics of the model cause the radius to be somewhat smaller over most of the depth range (see below). All models also include the α–β–γ transformations of olivine, whose effect is a reduction of temperature and density (for decreasing pressures/depths). For the convection melting models considered here, the principal effect of the olivine transformations is an acceleration of the upwelling plume at intermediate depths.

As described in more detail below and in Paper 2, the field observables considered in this study—namely crustal thickness, seismic velocities and electrical conductivities—are particularly sensitive to variations in temperature and melt content, which itself is also dependent on T. Therefore it is of substantial interest to investigate the effect of different temperatures and melt contents on these observables. With consideration of previous estimates for the temperature anomaly beneath Iceland and geochemical constraints on mantle porosities, our runs explore the parameter space given by $\Delta T_P(z_c) = 150$ K, 250 K and 350 K and by $\varphi_{ex} = 0.001$, 0.01 and 0.03 (runs 50-1, 135-1, 220-1, 135-0.1, 135-3 respectively; see Table 2), taking the intermediate values as a reference model; additionally, an unrealistic model 135-100 without melt segregation and extraction ($\varphi_{ex} = 1$) was also considered in order to force a strong magnetotelluric response and pronounced effect on seismic velocities due to the melt. To assess the importance of the background potential temperature, another run was made with parameters as for the reference model but with $T_{pot} = 1380\,^\circ$C (135-1c). Note that the model naming scheme is based on (rounded) ΔT_P values at a depth of 200 km (*cf.* Table 2); this is a convenient reference depth we will use in some more instances below, because it is more representative than the model bottom for the depth range covered by many regional observations which will be considered in Paper 2.

Some of the key variables discussed in the following, for example the maximum crustal thickness, h_{max}, the vertical upwelling velocity, $v_{s,z}$, and the buoyancy of the plume are estimated for a 'steady state'; however, in most models, no real steady state is reached. Therefore, we define the steady state to be represented by a stage in the evolution of the model in which the plume has already spread significantly under the lithosphere. This situation is usually reached after 20–22 Myr model time, as is obvious from the $h_{max}(t)$ plot in Fig. 1; most variables do not seem to vary appreciably at that stage any more. Further model parameters are listed in Table 1. Of the mentioned observables, the crustal thickness, which is the focus of this paper, is the most immediate outcome of the numerical models; on the other hand, it is quite well constrained to lie at 6–7 km according to seismic measurements, with a tendency to be thinner at half-spreading rates below about 1 cm yr^{-1} (e.g. White *et al.* 1992; Schubert *et al.* 2001). Hence, the spreading rates around Iceland are close to this limit, and without the influence of the plume, a crustal thickness slightly below the normal values would be possible.

2.2.1 The dynamic plume reference model (DPRM)

As a starting point for the exploration of the parameter space spanned by the plume excess temperature at the model bottom, ΔT_P, and the melt extraction threshold, φ_{ex}, we have defined a dynamic plume reference model (DPRM) and vary ΔT_P and φ_{ex}, which is equal to the highest stable porosity that can be reached in the model, in the different models. The model parameter combination of the

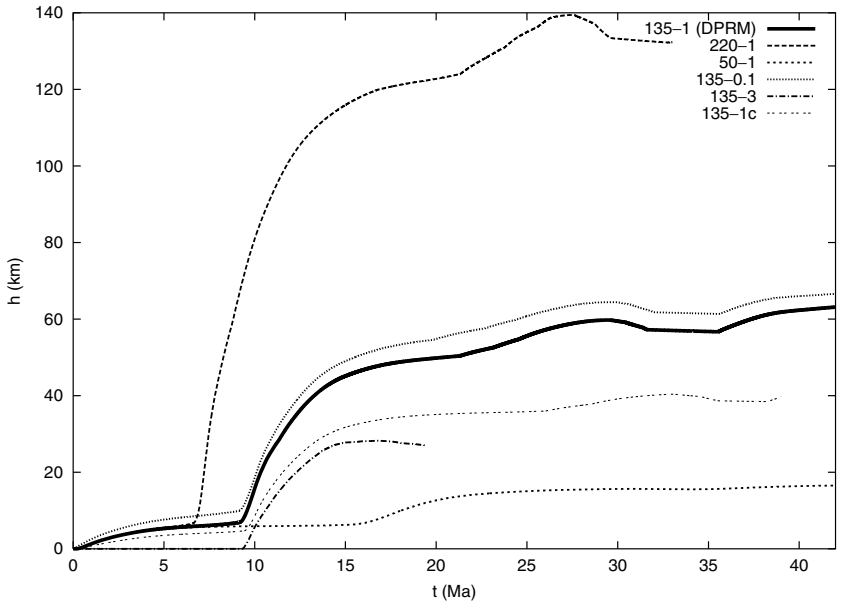

Figure 1. Maximum crustal thickness in the model as a function of time.

DPRM itself has been tuned to reproduce the thickness of normal oceanic crust and result in an anomalous plume-generated crustal thickness which should at least lie reasonably close to expected values. With respect to the Iceland plume, we chose $\Delta T_\mathrm{P} = 250$ K at the model bottom for the DPRM. This yields a plume temperature well within the range of current upper-mantle temperature estimates for this plume, because the plume cools during ascent. Although it is commonly accepted that melting in the mantle is near fractional, an adequate choice of the extraction threshold is even more difficult: while some argue for extremely low φ_ex of 10^{-3} or even less (e.g. McKenzie 1985), others claim that the permeability is far too low at such low porosities to allow for significant segregation and favour higher values like $\varphi_\mathrm{ex} \approx 0.02$–$0.03$ for the onset of efficient melt separation (Faul 2001). As a compromise, we chose $\varphi_\mathrm{ex} = 0.01$ for the DPRM (run 135-1).

The DPRM plume starts at the model bottom with $\Delta T_\mathrm{P} = 250$ K in its centre and crosses the solidus after about 9.2 Myr at a depth of about 110 km, having lost about half of its excess temperature; the temperature distribution of this model and the temperature contrast of the plume to the background mantle in the region covered by the melting grid are shown in Figs 2(a) and (b). During its ascent through the upper mantle, the central part of the plume accelerates in the zone of the olivine phase transitions, causing the conduit to thin to some extent as a consequence of mass conservation (Fig. 2a), and then slows down again when approaching the lithosphere. Apart from the decrease in viscosity and the increase of thermal expansivity to shallower depth throughout the depth range of the model, the reason for the increase in ascent velocity is the significant additional buoyancy caused by the fact that the lower-density α phase is formed in the hot plume at a somewhat greater depth than in the normal mantle, whereby the density contrast and concomitant buoyancy increase with plume temperature (Fig. 3). Above the transition zone, the effect disappears, as can be seen from the reduction in v_z and the localization of the phase-related buoyancy in Fig. 3. While the buoyant effect of the transition zone certainly has an effect on ascent velocity in the deep upper mantle, and therefore also on the shape and diameter of the plume; its immediate influence wanes towards the shallower parts of the mantle, so that its effect on the melting processes is minor. The non-thermal buoyancy components in the melting zone are mostly related to the depletion. The buoyancy related to retained melt is only of some importance at those depths of the plume's melting zone where normal mantle is still solid and causes a deep local maximum of the buoyancy at a depth of about 100 km, whereas above that level the porosity is virtually the same in the plume head and beneath the normal ridge due to the imposed extraction threshold (Fig. 3).

A further temperature drop of about 60 K is due to melting enthalpy and leads to a slight increase in viscosity in the whole melting region of up to about 0.2 log units. The temperature drop makes the plume head almost invisible in the temperature field in Fig. 2(a), but by subtracting the temperature at the model margin, $T(x, 0, z)$, from $T(x, y, z)$ (Fig. 2b), one can distinguish some details of the internal temperature structure of the thermal anomaly of the plume head. The onset of melting is marked by a decrease of the temperature anomaly above a depth of about 110 km, because melting is restricted to the plume there and the consumption of latent heat causes its temperature to approach that of the normal mantle. At about mid-depth of the melting model, at 75 km, the reference mantle beneath normal mid-oceanic ridges (MORs) also begins to melt and cool, so that the temperature contrast increases again to smaller depths because the melt productivity of the strongly depleted plume head in the shallowest parts of the melting region is lower than that of the less depleted sub-MOR mantle at a given z due to the concave-down shape of $f(\tilde{T})$.

As in most of our models, the vertical velocity of the plume peaks shortly below the top of the transition zone. It decreases to a somewhat constant lower value for the next 200–250 km, because the melting-related buoyancy increase at shallow depths counteracts the slowdown of the rising mantle and because the decrease of viscosity from (5–6.5) $\times$ 10^{19} Pa s at the plume axis in the transition zone to about 3.5 $\times$ 10^{19} Pa s just below the solidus depth and the reduction of thermal buoyancy due to cooling of the plume compensate to some extent. v_z then drops to values of a few cm yr^{-1} in the uppermost 100 km of the mantle (Fig. 3), where the plume head gets slightly stiffer, spreads laterally and starts to develop a lobe ring. At a depth of 100–150 km it already forms a small

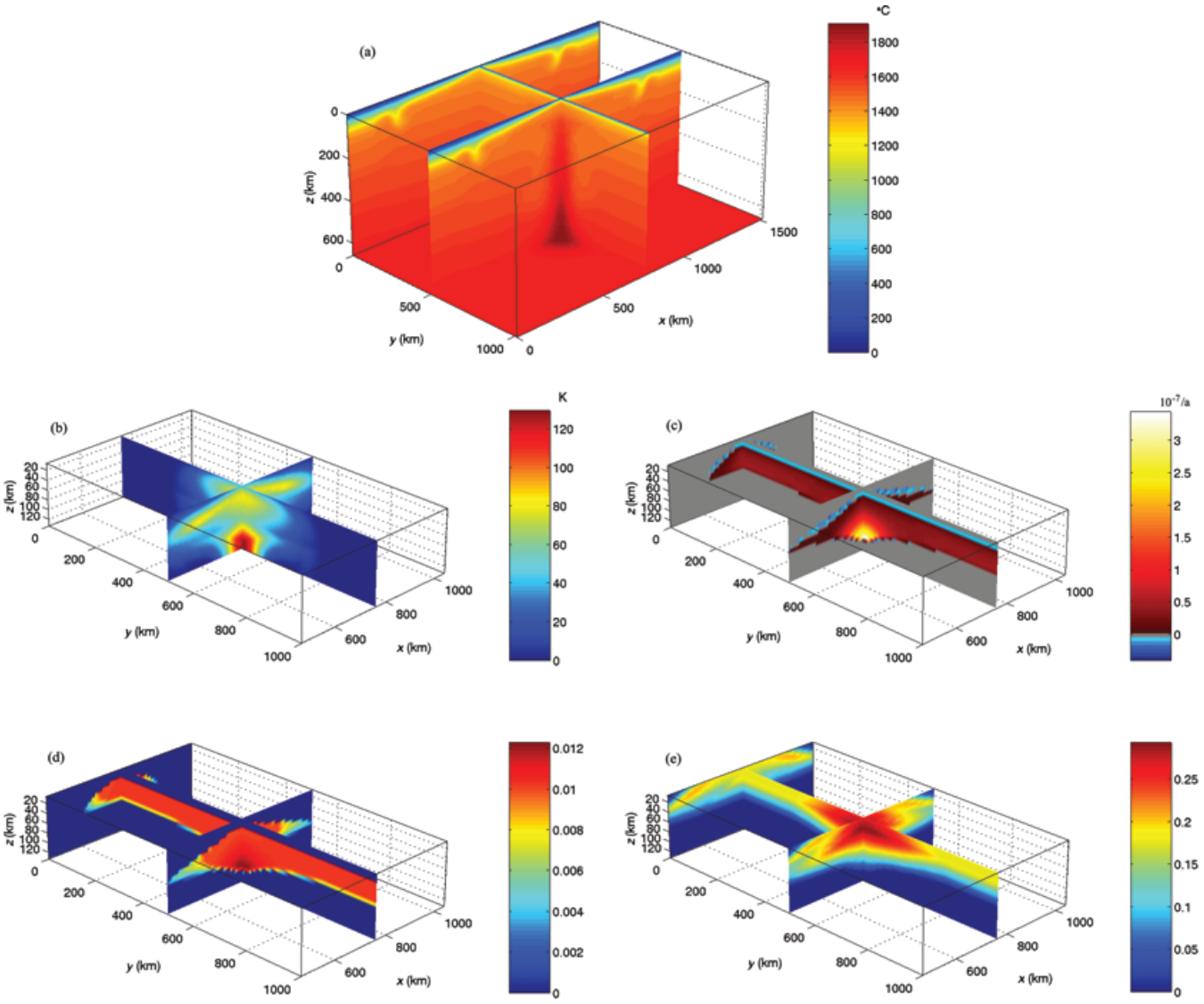

Figure 2. The DPRM at $t = 21$ Myr. (a) Temperature field in convection grid (in °C). (b) Temperature anomaly $T(x, y, z) - T(x, 0, z)$ in the melting grid (in K). (c) Melt production rate in the melting grid (in 10^{-7} yr^{-1}; negative values indicate freezing). (d) Melt fraction before extraction in the melting grid. (e) Degree of melting (depletion) field in the melting grid. The high-f zones at the outer margin of the depleted zone in (e) are remnants from the initial melting event in the first few time steps.

head, which is then slightly thicker than the stem; this is a feature which has also been observed by other workers (e.g. Feighner *et al.* 1995) and is probably related to both the slowdown of the plume when approaching the cold boundary layer and the influence of the flow field of the spreading plates. In the plume centre, T does not change significantly after 16 or 17 Myr, i.e. some 7 Myr after the plume head has begun to produce melt. In the first phase of plume–ridge interaction, there is a visible, though not strong, elongation of the upper part ($z \lesssim 45$ km) of the plume head along the ridge, but after some million years drag by the plates takes over control of the head's shape and extends the thermal anomaly perpendicularly to the ridge. Inspection of the thermal anomaly field suggests that a waist of some 400 km forms. For channelling of plume material into the ridge larger viscosity contrasts would be necessary (Albers & Christensen 2001) but cannot be reached with our algorithm. Thermal erosion of the lithosphere by the spreading plume head is not strong.

Figs 2(c) and (d) give an overview of the spatial distribution of melting. At the top of the model, normal MOR melting takes place continuously in the roughly triangular area beneath the ridge between depths of about 20 and 75 km. It is about 250 km wide at its base under normal ridge but broadens to more than 450 km during the spreading of the plume head and narrows only slightly at the later stages of plume evolution. The normal melting produces a layer of lighter depleted material beneath the lithosphere which moves to the sides, replacing the undepleted mantle (Fig. 2e); the high-f zones at the outer margin of the depleted zone are remnants from the initial melting event in the first few time steps. Degrees of melting in this layer reach a roughly constant level of around 18 per cent at intermediate depths. The plume starts to melt at around 9.2 Myr model time at a maximum depth of about 110 km and achieves a stronger depletion of 25–29 per cent in its central parts; the additional thermal and depletional density reduction in the plume enhances the upwelling in the melting zone, whereas the buoyant effect of retained

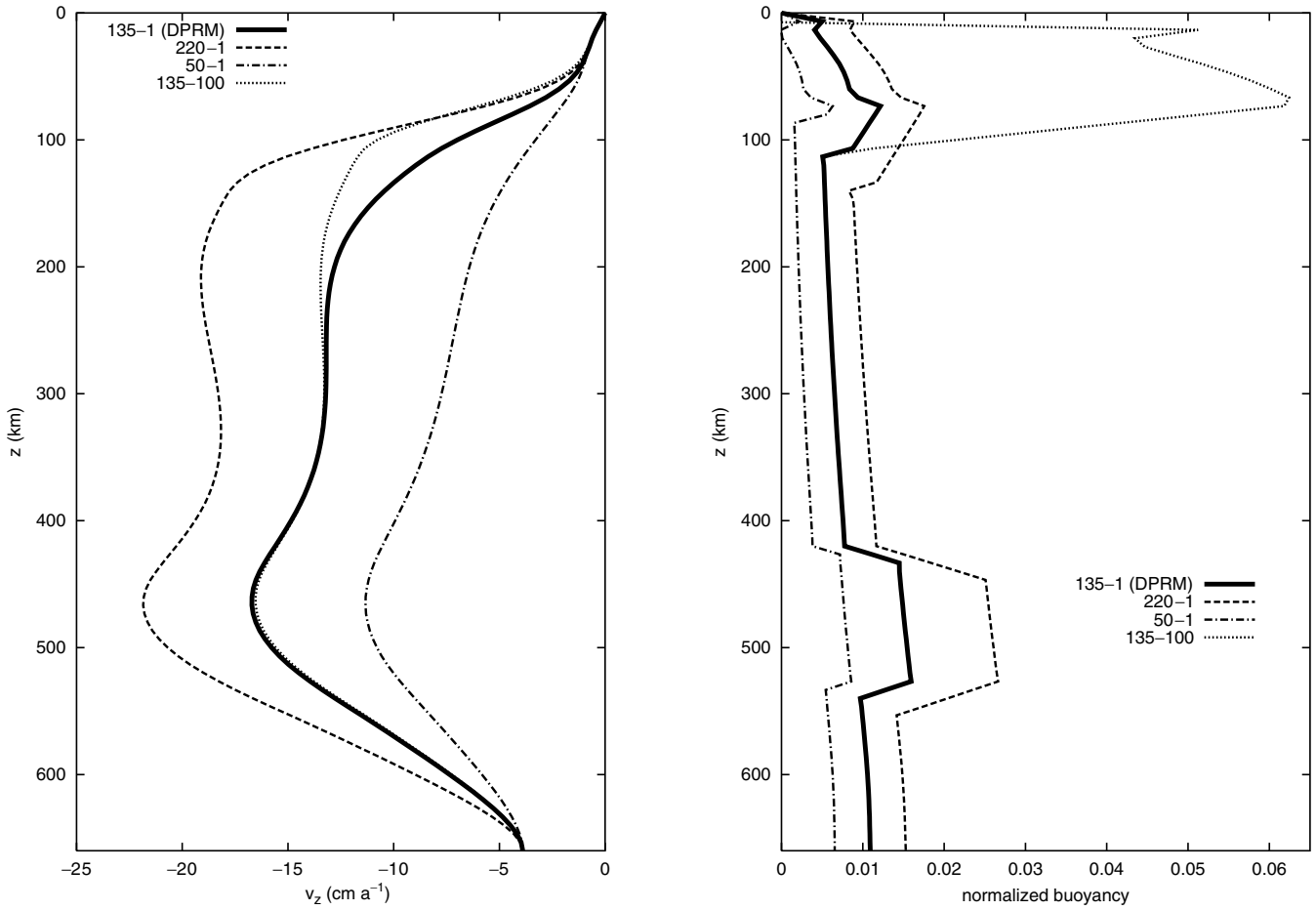

Figure 3. Selected $v_z(z)$ (left) and buoyancy (right) profiles through the plume centre at model times where crustal production has reached a quasi-steady state (30 Myr for 50-1, 21 Myr for the other models; see Fig. 1). The $v_z(z)$ profiles of models 135-0.1, 135-3 and 135-1c do not differ appreciably from the DPRM profile and have therefore been omitted. Note the pronounced deviation of 135-100 from the DPRM, which is due to the strong contribution of retained melt to buoyancy ($\varphi_{\max} \approx 0.3$). The buoyancy has been computed relative to a mantle profile at normal ridge, and has been normalized with $-g\varrho_0$.

melt is smaller and restricted to the deeper part of the plume head (Fig. 3). As one would expect from the melting parametrization of McKenzie & Bickle (1988) used in this study, melt production is largest in the initial stage of melting, thus most melts come from greater depths, especially those of the plume (Fig. 2c); higher temperatures and flow velocities cause the maximum melt production rate to be five to seven times higher in the plume head than beneath normal ridge, but the stronger depletion and accordingly decreasing $df/d\tilde{T}$ lead to a slightly lower rate of melting in the top of the plume head. Vertical segregation velocities of the retained melt are around 2–2.5 cm yr^{-1} as a maximum in both the plume head and beneath normal ridge; this is due to the prescribed threshold value which also causes the distribution of retained melt in the melting region to be quite homogeneous (Fig. 2d). Between the melting zone and the thermal lithosphere, a thin freezing layer exists where the mantle is being re-enriched by crystallization of retained melt (negative values in Fig. 2c).

The extracted melts form a crust of 5.6 km at normal ridge, which is only slightly below the range of observed values (White *et al.* 1992; Schubert *et al.* 2001) and therefore serves to calibrating the model. As can be seen from plots of the maximum crustal thickness in the model at a given time (Fig. 1), $h_{\max}(t)$, crustal growth rates are largest at the beginning of melting—both at the beginning of the model run and at the beginning of plume melting—and approach a steady-state value after some million years. For the DPRM, this value is 49 km, i.e. a bit larger than the maximum estimates of 39–46 km for the crust to the northwest of Vatnajökull in central Iceland as derived from the data from the ICEMELT and HOTSPOT projects (Darbyshire *et al.* 1998, 2000; Du & Foulger 2001; Allen *et al.* 2002b). The late-stage variability in crustal thickness and some other model variables are due to boundary effects of the model and will not be considered further.

2.2.2 Other models

All runs are summarized in Table 3. In runs 50-1 and 220-1, the melt extraction threshold has been kept at 1 per cent but the basal excess temperature of the plume has been changed to 150 K and 350 K, respectively. The cold plume 50-1 ascends quite sluggishly due to its smaller thermal buoyancy and slightly higher viscosity, cools more strongly and begins to melt later and at a shallower depth; its $v_{s,z}(z)$ profile is somewhat different from that of hotter plumes in that it lacks the constant interval in the upper half due to the comparatively small extent of melting and the related contributions to buoyancy (see Fig. 3), but nonetheless its buoyancy profile, while

Table 3. Model results. $\Delta T_P(z_{sol})$ is taken at the centreline of the plume. The maximum values of $v_{s,z}$ are estimated averages of the steady state. $v_{seg,z}$ for 135-100 is a rough estimate based on Darcy's law.

	h_{max} (km)	z_{sol} (km)	$\Delta T_P(z_{sol})$ (K)	Δz_X (km)	Max. $v_{s,z}$ (cm yr^{-1})	Max. $v_{seg,z}$ (cm yr^{-1})
Plume centre						
DPRM (135-1)	49	110	115	15	17	∼2.6
220-1	119	133	∼180	20	22	3.3
50-1	15	85	∼40	∼5	11	2.4
135-0.1	54	110	115		∼16	∼0.23
135-3	27	110	115	15	16	18
135-100	n.d.	110	115	15	∼16	O (km d^{-1})
135-1c	34	∼100	115	15	17	∼2.5
Normal ridge						
DPRM	5.6	75	–	–	∼1	∼2.5
135-0.1	7.7	75	–	–	∼1	∼0.08
135-3	0	75	–	–	∼1	9.5
135-1c	4	65	–	–	∼1	∼2.5

less markedly shaped, has the same structure as that of the DPRM. The maximum melting degree is only 23 per cent, and the final plume crust is no more than 15 km thick. As a whole, it is a rather unspectacular structure. By contrast, the hot plume 220-1 rises faster than the others due to its larger thermal and phase-related buoyancy and lower viscosity, which lies between about 2.5×10^{19} and 4×10^{19} Pa s, and crosses the solidus earlier and at greater depth, still with two-thirds of its bottom temperature excess in the centre; due to the deeper onset of melting, a larger depth interval is influenced by the buoyancy of retained melt than in the cooler plumes. The greater solidus depth will also make this plume the one whose melt productivity is influenced most by the speed-up experienced in the transition zone, although even here the effect is not dominant. However, the more extensive melting leads to stronger enthalpic cooling and lets the temperature contrast with the background mantle drop to only about 100 K at $z < 75$ km. The maximum degree of melting of more than 30 per cent is probably unrealistic because the expected exhaustion of clinopyroxene would reduce the productivity more strongly than modelled here.

The same threshold has been used for model 135-1c (cooler background T_{pot}). In that run, a cooler background temperature also means that the absolute temperature of the plume is lower than that of the DPRM by the corresponding amount. Generally speaking, one would expect this model to be a lower-performance clone of the DPRM in terms of melting, because the downward shift of the mantle geotherm shrinks the melting regions of both normal ridges and the plume and moves the solidus depth to a shallower level. Indeed, all geotherm–solidus intersections lie roughly 10 km higher, plume melting starts slightly later, the melting degrees are 2–3 per cent lower and the transition path of the material through the melting region is shorter, all of which lead to a noticeably thinner crust (Fig. 1).

The other variable parameter of this study, the threshold porosity φ_{ex}, was changed to 0.1, 3 and 100 per cent (no extraction), respectively, in models 135-0.1, 135-3 and 135-100; ΔT_P at the bottom was kept at 250 K. Dynamically, 135-0.1 and the DPRM 135-1 are very similar, because in both cases the retained amount of melt is quite low and therefore has only a minute effect on the buoyancy, visible near the solidus intersection. The main difference is the crustal thickness: the final MOR crust thickness is 7.7 km in 135-0.1, and the final plume crust thickness 54 km. The reason is obviously that in 135-0.1 almost all melt is extracted from the whole melting zone, whereas in the DPRM case a certain fraction, especially in the outer parts of the zone, hardly segregates and never makes it to the top but is rather transported outward and refreezes; moreover, as nearly everything is extracted in 135-0.1, there is hardly any melt left which would recrystallize later. By contrast, in run 135-3, all melt is retained under normal MOR, so that only the plume produces a crust; a plume with a bottom excess temperature of about 45 K, respectively 3–4 K at 200 km depth, is the weakest feature that would produce a crust with the other parameters unchanged (Fig. 4). Freezing rates at the melting zone margins are accordingly higher, and the freezing layer is thicker at the plume. The dynamic buoyancy effect of the melt relative to the DPRM is still small in this model. In the

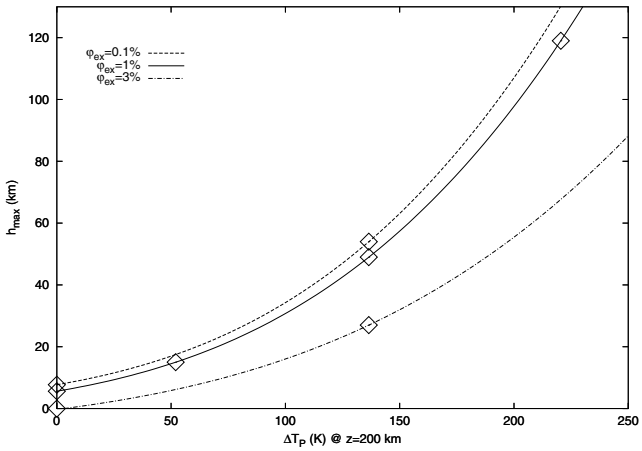

Figure 4. Maximum steady-state crustal thickness as a function of $\Delta T_P(z = 200$ km) and φ_{ex}, for a background mantle T_{pot} of 1410 °C. Within the given data range, the formula $h_{max} = (4.24 \times 10^{-6}\Delta T_P^3 + 8.25 \times 10^{-4}\Delta T_P^2 + 0.126\Delta T_P + 5.6)(-0.038\varphi_{ex}^2 - 0.07\varphi_{ex} + 1.11) + 1.698(1 - \Delta T_P/136.5)(1 - \varphi_{ex})$ km with ΔT_P in K and φ_{ex} in per cent can be used to approximate h_{max}; of course, $h_{max} \equiv 0$ where the formula yields negative values. This formula should not be used for extrapolation much beyond the data range, because limiting effects such as clinopyroxene exhaustion are expected at very high ΔT_P. The data points of all runs from Table 3 except 135-100 and 135-1c have been used for fitting. The formula was constructed by: (1) finding the cubic polynomial in ΔT_P through the points with $\varphi_{ex} = 1$ per cent; (2) finding the quadratic polynomial in φ_{ex} through the points with $\Delta T_P = 136.5$ K; (3) deriving the ΔT_P–φ_{ex}-dependent correction term to fit the h_{max} values of the DPRM and 135-0.1 at normal MOR ($\Delta T_P = 0$ K).

unrealistic last model 135-100, where all melt is retained, the melt finally has a large effect on buoyancy, which is expressed by the huge maximum at depths smaller than 100 km in the buoyancy plot of Fig. 3: in agreement with the depletion, porosities of more than 25 per cent are reached and accelerate the plume by 20–50 per cent in the depth range from about 200 to 50 km; the velocity would be even greater if the effect of melt on viscosity had been included, which would be necessary at such high porosities (e.g. Kohlstedt *et al.* 2000). On the one hand, the porosity-related buoyancy of the plume in model 135-100 affects mantle regions beneath the melting zone in that the increase in buoyancy counteracts the general tendency for reduced upwelling, but it is also effective throughout the melting region in this case, because the plume produces more melt than the MOR melting region and is not artificially reduced in this model; the effect on upwelling velocity, however, is damped by the proximity of the cool lithosphere and by the actual viscosity increase in the melting zone. For numerical reasons, segregation was not considered in this run.

An important general result of the models is shown in Fig. 4, where the quasi-stationary crustal thicknesses of the models (except 135-100 and the 'cold' model 135-1c) are plotted as a function of ΔT_P at a depth of 200 km. The principal feature of this plot is the strong non-linearity of $h(\Delta T_\mathrm{P})$, which is a result of the combined effect of the supersolidus temperature, active upwelling of the plume and the geometry of the melting region.

3 DISCUSSION

3.1 General/MOR melting model

One of the most important quantities for the validation of the models is the rather well-constrained crustal thickness h, and in particular the thickness of normal oceanic crust can serve to judge how realistic the background mantle in the model is. As can be seen from the summary in Table 3, the normal DPRM matches the constraint quite well by construction, whereas the model with a lower background mantle potential temperature results in values which are too low. Run 135-0.1, with a lower extraction threshold, in turn produces slightly too much crust. Thus, there is a trade-off between T_pot and φ_ex, but the whole data set suggests that T_pot in the range from about 1350 °C (White & McKenzie 1995) to 1400 °C, combined with extraction thresholds of a few tenths of a per cent would give reasonable results, in agreement with independent estimates (Lundstrom *et al.* 2000; Faul 2001). The models do not support the retention of melt fractions substantially larger than 1 per cent.

However, some caveats are necessary when considering these values. First, the phase transitions of the Al-bearing phase, in particular the spinel–garnet transition at a depth of about 80 km, have not been included for the sake of simplicity, although they will influence melting by slightly lowering the geotherm at shallower depths (e.g. Phipps Morgan 1997). However, its importance will depend on the depth of initial melting and the extent of garnet exhaustion, and is probably minor or nil, especially in the plume, which certainly starts melting in the garnet stability field. Besides, its effect on buoyancy is unclear: Scott & Stevenson (1989) did not find a significant influence of the spinel–garnet transition, whereas Niu & Batiza (1991) think that it does have a relevant effect. Second, the melting enthalpy, which is of substantial importance for the amount of melt produced, is not well constrained (Hess 1992; Hirschmann *et al.* 1999), but may introduce further ambiguity in addition to the T_pot–φ_ex trade-off. Third, we calculated $f(\tilde{T})$ with the widely used parametrization of McKenzie & Bickle (1988), which is concave-down at the low to moderate $\tilde{T}$ in the mantle; however, theoretical investigations (Asimow *et al.* 1997) and some experiments (Walter & Presnall 1994; Schwab & Johnston 2001) showed that concave-up $f(\tilde{T})$ are also possible, and such a curve would lead to a different spatial depletion and porosity pattern and maybe also to a different crustal thickness. Finally, we also assumed purely anhydrous melting and a homogeneous peridotitic mantle source; both assumptions are likely simplifications, and mainly the latter might cause melt productivity to be underestimated, especially if the plume contains some old recycled oceanic crust, as proposed for the Iceland plumes in several geochemical studies (e.g. Hanan & Schilling 1997; Chauvel & Hémond 2000; Scarrow *et al.* 2000; Korenaga & Kelemen 2000; Breddam 2002). In contrast, the volumetric contribution of possible hydrous initial melting is not thought to be substantial, because practically all water enters the melt at an early stage, rendering melting anhydrous already at low f (Nicolas 1990; Kushiro 2001). The presence of water and its loss upon melting, which was not considered in this study, also affects the viscosity of the mantle, because the dehydrated mantle would be much stiffer than the unmolten, and lowest viscosities would be reached not within the melting zone but rather directly below it (Hirth & Kohlstedt 1996); however, at normal mid-ocean ridges, where decompression melting is controlled by passive upwelling, the change in viscosity would have no direct impact on melting.

3.2 Plume dynamics

With the results for the normal oceanic crust in mind, the plume crust can now be considered. In the following, a crustal thickness of 35–41 km will be assumed to be realistic for the central part of Iceland, especially above the plume (Darbyshire *et al.* 2000). The hottest plume, run 220-1, can then be discarded at once, because it produces far too much crust. This plume is most similar to the narrow plume models of Ribe *et al.* (1995) and Ito *et al.* (1996) and the anhydrous model of Ito *et al.* (1999), which also produced an exceedingly thick crust; the even greater values of more than 250 or 300 km reached by them are partly to be attributed to their higher temperatures, partly to their different melting degree parametrization and partly to the fact that they use rheological laws which result in viscosities in and near the melting region lower by a factor of three to four than those even in model 220-1, so that the mass flux through the melting zone is higher in their models. By contrast, the coolest plume, run 50-1, produces too little crust, and will not generate substantially more at a lower extraction threshold (Fig. 4). The other models, though, fall into a range of values which require a closer look. At first sight, the DPRM and 135-0.1 also seem to be too productive, whereas 135-1c and 135-3 come closest to the observed h_max for the plume. However, accepting 135-3 would require us to use a lower φ_ex for the normal crust, which would otherwise be absent, but there is no obvious reason to do that. By contrast, 135-0.1 yields slightly too large a thickness for normal oceanic crust due to the low extraction threshold, making it a less than ideal candidate as well.

On the other hand, the thicker plume crust resulting from the DPRM does not necessarily invalidate those models, because in these values some simplifications of the models are inherent. For instance, exhaustion of clinopyroxene from the source rock would lead to strongly reduced melt production and is expected for the largest degrees of melting in the plume, but it has not been included in the present models. The most significant effects of such a

criterion would be a thinner crust above the plume and a possibly also a deeper top of the melting region, but as the 'clinopyroxene-out' limit will be exceeded only in a limited region and not very far, the effect is not expected to flatten the anomalous crust to a great extent, given that a certain reduction of the productivity is also inherent in the f parametrization. We did not implement, either, the possibility that the thick crust above the plume centre would thin by creep, as proposed by Buck (1996), but a rough estimate indicates that even a fairly cold, high-viscosity lower crust would thin by several kilometres over some million years, although there is some uncertainty in estimating the reference viscosity of the crust. These two effects could lower the $h_{\max}$ values of the DPRM to those observed in real data as in the Moho map of Darbyshire *et al.* (2000, Fig. 18b), both above the plume centre and away from the volcanic zones. Another issue is the aforementioned problem that our algorithm cannot handle viscosity variations large enough to allow for channelling of the melting plume head along the ridge axis; however, such a mechanism would probably decrease the maximum thickness, because the melt-producing material is distributed along a larger part of the spreading centre.

The difference between reality and the model restricted by these factors can be illustrated by comparing the spatial distribution of the calculated crust plotted in Fig. 5 with the Moho map of Darbyshire *et al.* (2000): while the width of Iceland is reproduced quite well, the along-ridge length, for example of the calculated crustal body thicker than 25 km, is only about two-thirds of the observed along-ridge extent of crust with a Moho deeper than 25 km, taken across Vatnajökull. It is to be expected that a plume with a greater radius and an accordingly larger volume flux such as the broad plume models of Ribe *et al.* (1995) and Ito *et al.* (1996) would approach the observed form better, although our plume models have a higher excess temperature than theirs. Furthermore, an increase of the viscosity due to dehydration would result in a deeper spreading of the melting plume head and also provide a means of distributing the melt over a larger ridge interval, as demonstrated by Ito *et al.* (1999), whose plume had a larger radius than ours at shallow depth. While an increase of r_{P} would probably improve the shape of the crust produced by the DPRM and similar models, and could also be held within the limits of seismological constraints to some extent, it would indicate that the volume flux estimates by Sleep (1990) or Schilling (1991) are too low; indeed, the plume of the dehydrated model of Ito *et al.* (1999) has a three to four times larger volume flux.

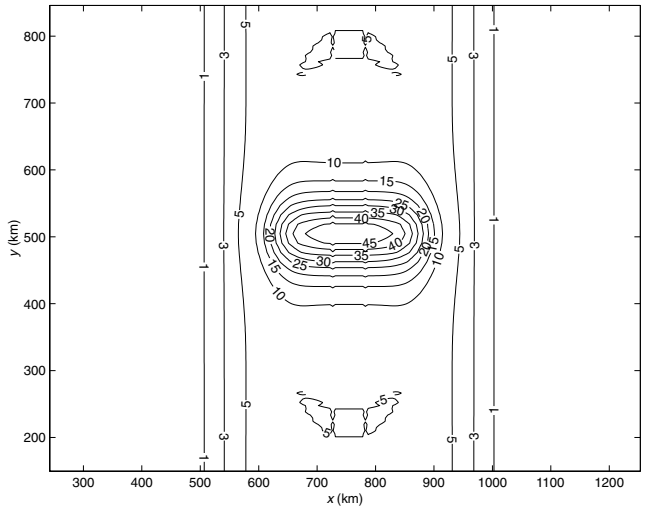

Figure 5. Calculated crustal thickness (in km) of the DPRM at 21 Myr model time. The two structures at $y \approx 220$ km and $y \approx 780$ km are weak artificial depressions. The ridge axis is located at $x = 750$ km, and is 60 km wide; plate drift has not yet transported crust further than about 210 km from it.

The effect of melting-induced dehydration is also another potentially important factor which would reduce the thickness of the anomalous crust, because the concomitant increase of viscosity strongly diminishes active upwelling of the plume, as shown by Ito *et al.* (1999). As pointed out above, moderate variability in viscosities can already contribute to substantial variation in maximum crustal thickness even in conventional p–T-dependent rheologies; the effect of water would introduce a much stronger change and make hotter plumes than the DPRM viable. However, the viscosity in most of the melting region of the model of Ito *et al.* (1999) with dehydration is significantly higher than independent viscosity estimates from field observations, which range from 3×10^{18} to 10^{19} Pa s (Sigmundsson 1991; Pollitz & Sacks 1996). Our models, whose viscosities lie between that of the dehydrated model of Ito *et al.* (1999) and the independent estimates, result in crustal thicknesses which are relatively close to those observed, or at least not as vastly different as the water-free ones from the previous studies of Ribe *et al.* (1995) and Ito *et al.* (1996, 1999). This shows that for a moderately hot plume like the DPRM, the match between modelled and observed h can already be improved to some extent with a slightly more viscous mantle, but that a strong additional mechanism such as the loss of water has probably to be invoked if the plume is much hotter than the DPRM. It also seems that the viscosity estimates from post-glacial rebound or post-seismic deformation cannot be applied directly to the stresses and timescales of mantle convection, probably because of the non-Newtonian behaviour expected in the melting zone (Karato & Wu 1993).

As an additional constraint for the temperature of the plume, geochemical estimates for the pressure and/or depth of initial melting can be used. Shen & Forsyth (1995) found a value of about 100 km for the Iceland plume, which would indicate a $\Delta T_{\mathrm{P}}(z = 200\ \mathrm{km})$ of about 100 K judging from the results in Table 3. The downward shift of the 410 km discontinuity relative to the undisturbed mantle, Δz_X, for a Clapeyron slope of about 2.9 MPa K^{-1} (Bina & Helffrich 1994) is also listed in Table 3 and can be compared with the results of Shen *et al.* (2002), who find a reduction of transition zone thickness of ∼19 km for the same Clapeyron slope at 410 km, corresponding to a temperature excess of at least 140 K. Our models do not include the effect on the 660 km discontinuity, but the Δz_X provide an upper bound for ΔT_{P}, because the Δz_X from the models cannot be larger than the total thinning of the transition zone, but should rather be about half that value. Therefore, a plume with a bottom ΔT_{P} between 200 and 250 K would fit the observation of Shen *et al.* (2002) best.

Furthermore, the ascent velocities of the plumes can be compared with independent estimates for the ratio of active to passive upwelling. For this upwelling ratio, values of 2–4 have been found in the depth range of melting (Holbrook *et al.* 2001; Allen *et al.* 2002b), but at the base of the melting region it might be as high as 10 (Maclennan *et al.* 2001; Kokfelt *et al.* 2003). These results are in good agreement with v_z at the plume axis in the DPRM and in models 135-0.1 and 135-1c, which corresponds to upwelling ratios of 7–8 at their respective solidus depths and drops to a ratio of 1 only near the top of the melting zone (see Fig. 3). In contrast, the hot plume of 220-1 has a ratio of 17 at the solidus depth, whereas the cold plume of 50-1 does not reach a ratio of more than ∼2.

The pronounced effect of active upwelling is also reflected by the superlinear increase of h with ΔT_P (Fig. 4), whose cause is that the amount of produced and extracted melt does not just depend straightforwardly on supersolidus temperature, but is also affected indirectly by consequences of a high ΔT_P. A hot plume also has a larger thermal (and depletion) buoyancy and a lower viscosity and therefore a larger flux of material processed in its melting zone, and the supersolidus part of the thermal anomaly affects a larger volume in the mantle, because melting starts at greater depth. Assuming that a large part of the melt from everywhere in the plume head is finally erupted at the spreading centre, the contribution of deep melts would be particularly large in hot plumes due to the geometry of the melting zone.

However, although the DPRM looks like the favourite within the framework of this series, it should be borne in mind that the trade-off between the effects of T_pot and φ_{ex} results in models 135-0.1 and 135-1c being not too bad either, because they indicate directions in which the parameter space is not well constrained. A further discussion of successful models will be given in Paper 2, where additional observables are considered.

3.3 Melt transport

The segregation velocity $\mathbf{v}_\mathrm{seg}$ depends strongly on the porosity of the rock, as can be seen from eqs (5) and (6). Therefore, variations in φ_ex have the strongest effect on $\mathbf{v}_\mathrm{seg}$: the maxima of $v_{\mathrm{seg},z}$ are on the order of 1 mm yr^{-1} for $\varphi_\mathrm{ex} = 10^{-3}$, around 2–3 cm yr^{-1} for $\varphi_\mathrm{ex} = 0.01$, essentially independent from T, and 10–20 cm yr^{-1} for $\varphi_\mathrm{ex} = 0.03$; for model 135-100, where segregation has not been modelled, $\varphi = 0.25$ would result in velocities on the order of kilometres per day. Similar ratios apply to the horizontal components of $\mathbf{v}_\mathrm{seg}$, but they are 1–2 orders of magnitude smaller, because melt flow is chiefly buoyancy driven. They reach their highest values in particular beneath the freezing front of the lithosphere, where the ascending melt is dammed and would form a high-φ layer, were it not extracted instantaneously; this layer, which was also observed by Ghods & Arkani-Hamed (2000) in a plain MOR model, would drain the melt towards the ridge. The low velocities justify the assumption that dissipation due to the relative motion of melt and matrix is negligible and that the average velocity of the partially molten rock can be approximated by $\mathbf{v}_\mathrm{s}$ as far as the transport of energy is concerned; the only model where this assumption might result in a minor underestimate of the temperature and melt production especially in the shallower parts of the melting zone is 135-3, but this does not affect the main conclusion regarding that model.

Although the values for v_seg are considered to be reasonable estimates of the order of magnitude of both absolute and relative segregation velocities, it should be kept in mind that there are several factors which were not included here, but which will have some impact on the velocity distribution of segregating melt; for example the viscosity of the melt, which is assumed constant in this study, actually depends on p, T and composition, which are all variable in the melting region, and may vary by 1.5 or 2 orders of magnitude over its depth range (Richet 1984; Kushiro 1986). It is therefore possible that the viscosity in the deeper parts of the melting zone is lowered strongly enough to (over)compensate the reduction of $v_{\mathrm{seg},z}$ due to the decrease in buoyancy of the compressed melt (Bagdassarov 1988). Unfortunately, the precise dependence of η_f on these variables is still poorly constrained and therefore difficult to include in a model. Furthermore, a φ-dependent bulk viscosity would probably increase the contribution of non-buoyancy terms to segregation (see eq. 5). The inclusion of water and dehydration and the resulting increase in viscosity would enhance the role of viscous deviatoric stresses in the focusing of melt towards the ridge (Braun *et al.* 2000); on the other hand, it would probably impede compaction.

4 CONCLUSIONS

We have conducted a series of numerical experiments on a simplified plume–ridge system in order to model the dynamics of plume ascent and melt generation in the present-day Iceland plume within the upper mantle. The dynamic convection and melting models yielded crustal thickness information for the plume and its surroundings which can be directly compared with observed values, but they also provide information on the distribution of temperature and melt content in the mantle, from which further predictions on other observables can be made; the latter is the subject of a companion paper (Paper 2).

Here, we restrict our judgment of the models to the reproduction of crustal thickness values observed in Iceland. Within the excess temperature-retained melt parameter space explored by our models we find that the model with a maximum excess temperature of 250 K at the bottom (136.5 K at $z = 200$ km, 115 K at the depth of the solidus) produces a plume crust quite close to the maximum crustal thickness observed in Iceland, given a background mantle potential temperature of 1410 °C; however, the along-axis extent of the anomalous crust is too small and requires some additional mechanism for the redistribution of the melting plume mantle under the ridge. Neither substantially higher fractions of retained melt nor much hotter plumes are allowed for by these models, whereas retained melt fractions lower by a few tenths of a per cent along with a plume cooler by a few tens of degrees would also be in agreement with observed crustal thicknesses. If the plume turns out to be significantly hotter, mechanisms such as melting dehydration would have to be invoked in order to reduce the strength of active upwelling in the melting region; the greater solidus depth might also make the enhanced upwelling of the plume in the phase transition region more important for the production of melts, at least in very hot and/or wet plumes. Plume excess temperatures around, or a bit less than, 200 K are also in agreement with previous numerical models (e.g. Ito *et al.* 1999), seismic tomography (e.g. Wolfe *et al.* 1997; Foulger *et al.* 2001; Allen *et al.* 2002a) and receiver function analysis (Shen *et al.* 2002). They are also in general agreement with the results from comparing predicted seismic velocities with observations (see Paper 2). Furthermore, the large values for the crust also support the notion that the Icelandic crust is thick.

Fig. 4 shows clearly that not only the excess temperature but also the amount of melt retained in the mantle and the extraction threshold φ_ex have a marked influence on crustal thickness, which has, in principle, several physical causes. The crucial point in our models is the limitation of the amount of melt that makes it to the crust. The buoyancy effect of retained melt, which enhances active upwelling, has some significance for dynamics only in the model without melt extraction (where no crust is formed, though). Our rheology law does not include the effect of retained melt, but experimental studies (e.g. Kohlstedt *et al.* 2000) suggest that at the low porosities prevailing in all of our models (except 135-100), the effect of retained melt on upwelling through the reduction of the viscosity is not important either.

Further conclusions from the dynamic models considering seismic and magnetotelluric measurements are drawn in Paper 2.

ACKNOWLEDGMENTS

We appreciate the constructive comments and suggestions of Gaël Choblet and an anonymous referee as well as the editor Yanick Ricard which have helped to clarify and enhance the discussion of several aspects. Most of this study was supported by research grants Schm 872/6-1, Schm 872/6-2, Ja 258/34-1, and Ja 258/34-2 of the Deutsche Forschungsgemeinschaft to TR, GM and AK.

REFERENCES

Aharonov, E., Whitehead, J.A., Kelemen, P.B. & Spiegelman, M., 1995. Channeling instability of upwelling melt in the mantle, *J. geophys. Res.,* **100**(B10), 20 433–20 450.

Albers, M. & Christensen, U.R., 2001. Channeling of plume flow beneath mid-ocean ridges, *Earth planet. Sci. Lett.,* **187,** 207–220.

Allen, R.M. *et al.,* 1999. The thin hot plume beneath Iceland, *Geophys. J. Int.,* **137**(1), 51–63.

Allen, R.M. *et al.,* 2002a. Imaging the mantle beneath Iceland using integrated seismological techniques, *J. geophys. Res.,* **107**(B12), 2325.

Allen, R.M. *et al.,* 2002b. Plume driven plumbing and crustal formation in Iceland, *J. geophys. Res.,* **107**(B8), 2163.

Asimow, P.D., Hirschmann, M.M. & Stolper, E.M., 1997. An analysis of variations in isentropic melt productivity, *Phil. Trans. R. Soc. Lond.,* A, **355**(1723), 255–281.

Bagdassarov, N.S., 1988. Accumulation capacity of spinel lherzolite partial melts, *Geokhimiya,* **8,** 1168–1176 (English translation published by Scripta Technica, 1989).

Beblo, M. & Björnsson, A., 1980. A model of electrical resistivity beneath NE Iceland, correlation with temperature, *J. Geophys.,* **47,** 184–190.

Bercovici, D., Ricard, Y. & Schubert, G., 2001. A two-phase model for compaction and damage. 1. General theory, *J. geophys. Res.,* **106**(B5), 8887–8906.

Bijwaard, H. & Spakman, W., 1999. Tomographic evidence for a narrow whole mantle plume below Iceland, *Earth planet. Sci. Lett.,* **166,** 121–126.

Bina, C.R. & Helffrich, G.R., 1994. Phase transition Clapeyron slopes and transition zone seismic discontinuity topography, *J. geophys. Res.,* **99**(B8), 15 853–15 860.

Bjarnason, I.Þ., Menke, W., Flóvenz, Ó.C. & Caress, D., 1993. Tomographic image of the mid-Atlantic plate boundary in southwestern Iceland, *J. geophys. Res.,* **98,** 6607–6622.

Bjarnason, I.Þ., Wolfe, C.J., Solomon, S.C. & Gudmundsson, G., 1996. Initial results from the ICEMELT experiment: body-wave delay times and shear-wave splitting across Iceland, *Geophys. Res. Lett.,* **23**(5), 459–462 (correction in *Geophys. Res. Lett.,* **23**(8), 903).

Braun, M.G., Hirth, G. & Parmentier, E.M., 2000. The effect of deep damp melting on mantle flow and melt generation beneath mid-ocean ridges, *Earth planet. Sci. Lett.,* **176,** 339–356.

Breddam, K., 2002. Kistufell: primitive melt from the Iceland mantle plume, *J. Petrol.,* **43**(2), 345–373.

Buck, W.R., 1991. Modes of continental lithospheric extension, *J. geophys. Res.,* **96**(B12), 20 161–20 178.

Buck, W.R., 1996. Shallow redistribution of crust produced by mantle plumes at mid-ocean ridges, in *European Seismological Commission, XXV General Assembly, Reykjavik, Iceland, Abstracts,* p. 117, Icelandic Meteorological Office, Reykjavik.

Cella, F. & Rapolla, A., 1997. Density changes in upwelling mantle, *Phys. Earth planet. Int.,* **103,** 63–84.

Chauvel, C. & Hémond, C., 2000. Melting of a complete section of recycled oceanic crust: trace element and Pb isotope evidence from Iceland, *Geochem. Geophys. Geosyst.,* **1,** 1999GC000002.

Courtial, P., Ohtani, E. & Dingwell, D.B., 1997. High-temperature densities of some mantle melts, *Geochim. Cosmochim. Acta,* **61**(15), 3111–3119.

Courtillot, V., Davaille, A., Besse, J. & Stock, J., 2003. Three distinct types of hotspots in the Earth's mantle, *Earth planet. Sci. Lett.,* **205**(3–4), 295–308.

Darbyshire, F.A., Bjarnason, I.Þ., White, R.S. & Flóvenz, Ó.G., 1998. Crustal structure above the Iceland mantle plume imaged by the ICEMELT refraction profile, *Geophys. J. Int.,* **135**(3), 1131–1149.

Darbyshire, F.A., White, R.S. & Priestley, K.F., 2000. Structure of the crust and uppermost mantle of Iceland from a combined seismic and gravity study, *Earth planet. Sci. Lett.,* **181,** 409–428.

Davis, B.T.C. & England, J.L., 1964. The melting of forsterite up to 50 kilobars, *J. geophys. Res.,* **69**(6), 1113–1116.

Du, Z. & Foulger, G.R., 2001. Variation in the crustal structure across central Iceland, *Geophys. J. Int.,* **145**(1), 246–264.

Falloon, T.J., Green, D.H., Hatton, C.J. & Harris, K.L., 1988. Anhydrous melting of a fertile and depleted peridotite from 2 to 30 kb and application to basalt petrogenesis, *J. Petrol.,* **29**(6), 1257–1282.

Faul, U.H., 2001. Melt retention and segregation beneath mid-ocean ridges, *Nature,* **410,** 920–923.

Feighner, M.A., Kellogg, L.H. & Travis, B.J., 1995. Numerical modeling of chemically buoyant mantle plumes at spreading ridges, *Geophys. Res. Lett.,* **22**(6), 715–718.

Foulger, G.R. *et al.,* 2001. Seismic tomography shows that upwelling beneath Iceland is confined to the upper mantle, *Geophys. J. Int.,* **146**(2), 504–530.

Gebrande, H., Miller, H. & Einarsson, P., 1980. Seismic structure of Iceland along RRISP-Profile I, *J. Geophys.,* **47,** 239–249.

Ghods, A. & Arkani-Hamed, J., 2000. Melt migration beneath mid-ocean ridges, *Geophys. J. Int.,* **140**(3), 687–697.

Grand, S.P., 2002. Mantle shear-wave tomography and the fate of subducted slabs, *Phil. Trans. R. Soc. Lond.,* A, **360**(1800), 2475–2491.

Green, D.H. & Falloon, T.J., 1998. Pyrolite: a Ringwood concept and its current expression, in *The Earth's Mantle—Composition, Structure, and Evolution,* pp. 311–378, ed. Jackson, I., Cambridge University Press, Cambridge.

Green, D.H., Falloon, T., Eggins, S.M. & Yaxley, G.M., 2001. Primary magmas and mantle temperatures, *Eur. J. Mineral.,* **13**(3), 437–451.

Hanan, B.B. & Schilling, J.-G., 1997. The dynamic evolution of the Iceland mantle plume: the lead isotope perspective, *Earth planet. Sci. Lett.,* **151,** 43–60.

Hanan, B.B., Blichert-Toft, J., Kingsley, R. & Schilling, J.-G., 2000. Depleted Iceland mantle plume geochemical signature: artifact of multicomponent mixing?, *Geochem. Geophys. Geosyst.,* **1,** 1999GC000009.

Hess, P.C., 1992. Phase equilibria constraints on the origin of ocean floor basalts, in *Mantle Flow and Melt Generation at Mid-ocean Ridges,* American Geophysical Union Geophysical Monograph 71, pp. 67–102, eds Morgan, J.P., Blackman, D.K. & Sinton, J.M., American Geophysical Union, Washington, DC.

Hirose, K. & Kawamura, K., 1994. A new experimental approach for incremental batch melting of peridotite at 1.5 GPa, *Geophys. Res. Lett.,* **21**(19), 2139–2142.

Hirschmann, M.M., 2000. Mantle solidus: experimental constraints and the effects of peridotite composition, *Geochem. Geophys. Geosyst.,* **1,** 2000GC000070.

Hirschmann, M.M., Asimow, A.D., Ghiorso, M.S. & Stolper, E.M., 1999. Calculation of peridotite partial melting from thermodynamic models of minerals and melts. III. Controls on isobaric melt production and the effect of water on melt production, *J. Petrol.,* **40**(5), 831–851.

Hirth, G. & Kohlstedt, D.L., 1996. Water in the oceanic upper mantle: implications for rheology, melt extraction and evolution of the lithosphere, *Earth planet. Sci. Lett.,* **144,** 93–108.

Hofmeister, A.M., 1999. Mantle values of thermal conductivity and the geotherm from phonon lifetimes, *Science,* **283,** 1699–1706.

Holbrook, W.S. *et al.,* 2001. Mantle thermal structure and active upwelling during continental breakup in the North Atlantic, *Earth planet. Sci. Lett.,* **190**(3–4), 251–266.

Ito, G., Lin, J. & Gable, C.W., 1996. Dynamics of mantle flow and melting at a ridge-centered hotspot: Iceland and the mid-Atlantic ridge, *Earth planet. Sci. Lett.,* **144,** 53–74.

Ito, G., Shen, Y., Hirth, G. & Wolfe, C.J., 1999. Mantle flow, melting and dehydration of the Iceland mantle plume, *Earth planet. Sci. Lett.,* **165,** 81–96.

Iwamori, H., McKenzie, D. & Takahashi, E., 1995. Melt generation by isentropic mantle upwelling, *Earth planet. Sci. Lett.,* **134,** 253–266.

Karato, S.-I., 1993. Importance of anelasticity in the interpretation of seismic anisotropy, *Geophys. Res. Lett.,* **20**(15), 1623–1626.

Karato, S.-I. & Wu, P., 1993. Rheology of the upper mantle: a synthesis, *Science,* **260,** 771–778.

Kempton, P.D., Fitton, J.G., Saunders, A.D., Nowell, G.M., Taylor, R.N., Hardarson, B.S. & Pearson, G., 2000. The Iceland plume in space and time: a Sr–Nd–Pb–Hf study of the North Atlantic rifted margin, *Earth planet. Sci. Lett.,* **177**(3–4), 255–271.

Kohlstedt, D.L., Bai, Q., Wang, Z.-C. & Mei, S., 2000. Rheology of partially molten rocks, in *Physics and Chemistry of Partially Molten Rocks,* pp. 3–28, eds Bagdassarov, N., Laporte, D. & Thompson, A.B., Kluwer Academic, Dordrecht.

Kokfelt, T.F., Hoernle, K. & Hauff, F., 2003. Upwelling and melting of the Iceland plume from radial variation of ^{238}U–^{230}Th disequilibria in postglacial volcanic rocks, *Earth planet. Sci. Lett.,* **214**(1–2), 167–186 (erratum in *Earth planet. Sci. Lett.,* **217** (1–2), 219–220).

Korenaga, J. & Kelemen, P.B., 2000. Major element heterogeneity in the mantle source of the North Atlantic igneous province, *Earth planet. Sci. Lett.,* **184**(1), 251–268.

Kreutzmann, A., Schmeling, H., Junge, A., Ruedas, T., Marquart, G. & Bjarnason, I., 2004. Dynamics and melting of a ridge-centered plume with application to Iceland. Part II: Predictions for electromagnetic and seismic observables, *Geophys. J. Int.,* submitted.

Kushiro, I., 1986. Viscosity of partial melts in the upper mantle, *J. geophys. Res.,* **91**(B9), 9343–9350.

Kushiro, I., 2001. Partial melting experiments on peridotite and origin of mid-ocean ridge basalt, *Ann. Rev. Earth planet. Sci.,* **29,** 71–107.

Lundstrom, C., 2000. Models of U-series disequilibria generation in MORB: the effects of two scales of melt porosity, *Phys. Earth planet. Int.,* **121,** 189–204.

Lundstrom, C., Gill, J. & Williams, Q., 2000. A geochemically consistent hypothesis for MORB generation, *Chem. Geol.,* **162**(2), 105–126.

Maclennan, J., McKenzie, D. & Grönvold, K., 2001. Plume-driven upwelling under central Iceland, *Earth planet. Sci. Lett.,* **194** (1–2), 67–82.

Marquart, G., 1991. Interpretation of geoid anomalies around the Iceland hotspot, *Geophys. J. Int.,* **106,** 149–160.

Marquart, G., 2001. On the geometry of mantle flow beneath drifting lithospheric plates, *Geophys. J. Int.,* **144**(2), 356–372.

Marquart, G., Schmeling, H., Ito, G. & Schott, B., 2000. Conditions for mantle plumes to penetrate the mantle phase boundaries, *J. Geophys. Res.,* **105**(B3), 5679–5694.

McKenzie, D., 1984. The generation and compaction of partially molten rock, *J. Petrol.,* **25,** 713–765.

McKenzie, D., 1985. ^{230}Th–^{238}U disequilibrium and the melting processes beneath ridge axes, *Earth planet. Sci. Lett.,* **72,** 149–157.

McKenzie, D. & Bickle, M.J., 1988. The volume and composition of melt generated by extension of the lithosphere, *J. Petrol.,* **29**(3), 625–679.

Menke, W., Brandsdóttir, B., Einarsson, P. & Bjarnason, I.Þ., 1996. Reinterpretation of the RRISP-77 Iceland shear-wave profiles, *Geophys. J. Int.,* **126,** 166–172.

Morgan, W.J., 1971. Convection plumes in the lower mantle, *Nature,* **230,** 42–43.

Navrotsky, A., 1994. *Physics and Chemistry of Earth Materials,* Cambridge University Press, Cambridge.

Nicolas, A., 1990. Melt extraction from mantle peridotites: hydrofracturing and porous flow, with consequences for oceanic ridge activity, in *Magma Transport and Storage,* pp. 159–173, ed. Ryan, M.P., Wiley, Chichester.

Niu, Y. & Batiza, R., 1991. *In situ* densities of MORB melts and residual mantle: implications for buoyancy forces beneath mid-ocean ridges, *J. Geol.,* **99,** 767–775.

Ohtani, E. & Kumazawa, M., 1981. Melting of forsterite Mg_2SiO_4 up to 15 GPa, *Phys. Earth planet. Int.,* **27,** 32–38.

Phipps Morgan, J., 1987. Melt migration beneath mid-ocean spreading centers, *Geophys. Res. Lett.,* **14**(12), 1238–1241.

Phipps Morgan, J., 1997. The generation of a compositional lithosphere by mid-ocean ridge melting and its effect on subsequent off-axis hotspot upwelling and melting, *Earth planet. Sci. Lett.,* **146,** 213–232.

Pollitz, F.F. & Sacks, I.S., 1996. Viscosity structure beneath northeast Iceland, *J. geophys. Res.,* **101**(B8), 17 771–17 793.

Presnall, D.C. & Walter, M.J., 1993. Melting of forsterite, Mg_2SiO_4, from 9.7 to 16.5 GPa, *J. geophys. Res.,* **98**(B11), 19 777–19 783.

Ribe, N.M., Christensen, U.R. & Theissing, J., 1995. The dynamics of plume–ridge interaction, 1: Ridge-centered plumes, *Earth Planet. Sci. Lett.,* **134,** 155–168.

Richet, P., 1984. Viscosity and configurational entropy of silicate melts, *Geochim. Cosmochim. Acta,* **48,** 471–483.

Richet, P., Leclerc, F. & Benoist, L., 1993. Melting of forsterite and spinel, with implications for the glass transition of Mg_2SiO_4 liquid, *Geophys. Res. Lett.,* **20**(16), 1675–1678.

Rigden, S.M., Ahrens, T.J. & Stolper, E.M., 1989. High-pressure equation of state of molten anorthite and diopside, *J. geophys. Res.,* **94**(B7), 9508–9522.

Ritsema, J., van Heijst, H.J. & Woodhouse, J.H., 1999. Complex shear wave velocity structure imaged beneath Africa and Iceland, *Science,* **286,** 1925–1928.

Ryabchikov, I.D., 1998. Geochemical modelling of magma generation in passive and active mantle plumes, in *Challenges to Chemical Geology,* pp. 103–120, eds Novak, M. & Rosenbaum, J., Czech Geological Survey, Prague.

Scarrow, J.H., Curran, J.M. & Kerr, A.C., 2000. Major element records of variable plume involvement in the north Atlantic province tertiary flood basalts, *J. Petrol.,* **41**(7), 1155–1176.

Schilling, J.-G., 1991. Fluxes and excess temperatures of mantle plumes inferred from their interaction with migrating mid-ocean ridges, *Nature,* **352,** 397–403.

Schmeling, H., 1985. Numerical models on the influence of partial melt on elastic, anelastic, and electric properties of rocks. Part I: elasticity and anelasticity, *Phys. Earth planet. Int.,* **41,** 34–57.

Schmeling, H., 1986. Numerical models on the influence of partial melt on elastic, anelastic, and electric properties of rocks. Part II: electrical conductivity, *Phys. Earth planet. Int.,* **43,** 123–136.

Schmeling, H., 2000. Partial melting and melt segregation in a convecting mantle, in *Physics and Chemistry of Partially Molten Rocks,* pp. 141–178, eds Bagdassarov, N., Laporte, D. & Thompson, A.B., Kluwer Academic, Dordrecht.

Schubert, G., Turcotte, D.L. & Olson, P., 2001. *Mantle Convection in the Earth and Planets,* Cambridge University Press, Cambridge.

Schwab, B.E. & Johnston, A.D., 2001. Melting systematics of modally variable, compositionally intermediate peridotites and the effects of mineral fertility, *J. Petrol.,* **42**(10), 1789–1811.

Scott, D.R. & Stevenson, D.J., 1989. A self-consistent model of melting, magma migration and buoyancy-driven circulation beneath mid-ocean ridges, *J. geophys. Res.,* **94**(B3), 2973–2988.

Shen, Y. & Forsyth, D.W., 1995. Geochemical constraints on the initial and final depths of melting beneath mid-ocean ridges, *J. geophys. Res.,* **100**(B2), 2211–2237.

Shen, Y. *et al.,* 2002. Seismic evidence for a tilted mantle plume and north–south mantle flow beneath Iceland, *Earth planet. Sci. Lett.,* **197**(3–4), 261–272.

Sigmundsson, F., 1991. Post-glacial rebound and asthenosphere viscosity in Iceland, *Geophys. Res. Lett.,* **18**(6), 1131–1134.

Sleep, N.H., 1990. Hotspots and mantle plumes: some phenomenology, *J. geophys. Res.,* **95**(B5), 6715–6736.

Staples, R.K., White, R.S., Brandsdóttir, B., Menke, W., Maguire, P. K.H. & McBride, J.H., 1997. Färoe–Iceland ridge experiment, 1, Crustal structure of northeastern Iceland, *J. geophys. Res.,* **102**(B4), 7849–7866.

Stevenson, D.J., 1989. Spontaneous small-scale melt segregation in partial melts undergoing deformation, *Geophys. Res. Lett.,* **16**(9), 1067–1070.

Tryggvason, K., Husebye, E. & Stefánsson, R., 1983. Seismic image of the hypothesized Icelandic hot spot, *Tectonophysics,* **100,** 97–118.

Turcotte, D.L. & Schubert, G., 1982. *Geodynamics—Applications of Continuum Physics to Geological Problems,* John Wiley, Chichester.

Walter, M.J. & Presnall, D.C., 1994. Melting behaviour of simplified lherzolite in the system $CaO–MgO–Al_2O_3–SiO_2–Na_2O$ from 7 to 35 kbar, *J. Petrol.,* **35**(2), 329–359.

White, R.S. & McKenzie, D.P., 1995. Mantle plumes and flood basalts, *J. geophys. Res.,* **100**(B9), 17 543–17 585.

White, R.S., McKenzie, D.P. & O'Nions, R.K., 1992. Oceanic crustal thickness from seismic measurements and rare earth element inversions, *J. geophys. Res.,* **97**(B13), 19 683–19 715.

Wolfe, C.J., Bjarnason, I.Þ., VanDecar, J. & Solomon, S., 1997. Seismic structure of the Iceland mantle plume, *Nature,* **385**(5727), 245–247.

Zhao, D., 2001. Seismic structure and origin of hotspots and mantle plumes, *Earth planet. Sci. Lett.,* **192**(3), 251–265.

Zverev, S.M., Litvinenko, I.V., Pálmason, G., Yaroshevskaya, G.A. & Osokin, N.N., 1980. A seismic crustal study of the axial rift zone in southwest Iceland, *J. Geophys.,* **47,** 202–210.

Zverev, S.M., Litvinenko, I.V., Pálmason, G., Yaroshevskaya, G.A., Osokin, N.N. & Akhmetjev, M.A., 1980. A seismic study of the rift zone in northern Iceland, *J. Geophys.,* **47,** 191–201.